analytical chemistry

pubs.acs.org/ac Article

# Oxidative Cleavage-Based Three-Dimensional DNA Biosensor for Ratiometric Detection of Hypochlorous Acid and Myeloperoxidase

Jing Wang, Jia-Yi Ma, Dong-Xia Wang, Bo Liu, Xiao Jing, Dan-Ye Chen, An-Na Tang, and De-Ming Kong*

Cite This: *Anal. Chem.* 2021, 93, 16231−16239 Read Online

ACCESS | Metrics & More | Article Recommendations | Supporting Information

**ABSTRACT:** Methods to detect and quantify disease biomarkers with high specificity and sensitivity in biological fluids play a key role in enabling clinical diagnosis, including point-of-care testing. Myeloperoxidase (MPO) is an emerging biomarker for the detection of inflammation, neurodegenerative diseases, and cardiovascular disease, where excess MPO can lead to oxidative damage to biomolecules in homeostatic systems. While numerous methods have been developed for MPO analysis, most techniques are challenging in clinical applications due to the lack of amplification methods, high cost, or other practical drawbacks. Enzyme-linked immunosorbent assays are currently used for the quantification of MPO in clinical practice, which is often limited by the availability of antibodies with high affinity and specificity and the significant nonspecific binding of antibodies to the analytical surface. In contrast, nucleic acid-based biosensors are of interest because of their simplicity, fast response time, low cost, high sensitivity, and low background signal, but detection targets are limited to nucleic acids and non-nucleic acid biomarkers are rare. Recent studies reveal that the modification of a genome in the form of phosphorothioate is specifically sensitive to the oxidative effects of the MPO/$H_2O_2$/$Cl^-$ system. We developed an oxidative cleavage-based three-dimensional DNA biosensor for rapid, ratiometric detection of HOCl and MPO in a "one-pot" method, which is simple, stable, sensitive, specific, and time-saving and does not require a complex reaction process, such as PCR and enzyme involvement. The constructed biosensor has also been successfully used for MPO detection in complex samples. This strategy is therefore of great value in disease diagnosis and biomedical research.

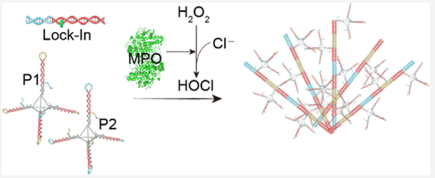




Pathological features of diseases are usually accompanied by the upregulation of certain biomarkers such as ions, nucleic acids, small molecules, and proteins. Detection tools with high sensitivity and compatibility are of great significance for the accurate diagnosis of diseases. However, the sensitivity, accuracy, and biosafety of probes remain challenging, which prompts researchers to explore more applicable materials and platforms to address these issues. Myeloperoxidase (MPO), a heme protease, is mainly derived from polymorphonuclear neutrophils and also exists in monocytes and macrophages. When phagocytosis is activated by inflammatory stimuli, a large amount of active MPO is secreted into the phagosome, catalyzing $H_2O_2$ and chloride ions ($Cl^-$) to produce high bactericidal HOCl. In addition to HOCl, MPO also catalyzes the formation of other reactive molecules such as aldehydes, tyrosyl radicals, hydroxyl radicals, and nitrite. Therefore, MPO is associated with severe infections and various inflammatory diseases such as cardiovascular disease, glomerular injury, rheumatoid arthritis, atherosclerosis, pulmonary fibrosis, Alzheimer's disease, Parkinson's disease, and certain cancers.[1,2] The determination of MPO plays a vital role in assisting the diagnosis of related diseases. Goldmann et al. found that MPO was significantly elevated within 2 h after the onset of chest pain symptoms in patients with acute myocardial infarction and could be detected, whereas cardiac troponin T, which is widely used clinically to determine cardiomyocyte damage, required 3−6 h after myocardial infarction. Therefore, the study of MPO and its enzymatic reaction systems has received extensive attention, especially in the biological and medical fields.

There are various methods for evaluating MPO activity, such as colorimetry,[3] radiometric assay,[4] electrochemistry,[5,6] chemiluminescence,[7−9] enzyme-linked immunosorbent assays,[10] fluorescence imaging,[11,12] magnetic resonance imaging,[13] and CT imaging.[14] Although most of the existing analytical methods have good specificity, they all suffer from some problems such as long detection time, limited sensitivity, complicated preparation process, or the need for large-scale equipment. MPO-mediated generation of HOCl, on the other hand, is considered a relevant biomarker of oxidative stress-related damage, and its qualitative and quantitative analysis is of great significance to the study of disease progression. Currently, several analytical methods have been established to detect HOCl.[15] Among them, fluorescent probes have been

**Received:** September 22, 2021
**Accepted:** November 16, 2021
**Published:** November 25, 2021




https://doi.org/10.1021/acs.analchem.1c04113
*Anal. Chem.* 2021, 93, 16231−16239

**Scheme 1. (a) HOCl Breaks PS-Modified Nucleic Acids at Specific Sites, (b) Illustration of the TDN-HCR Platform for the Detection of HOCl, and (c) Illustration of the TDN-HCR for the Detection of MPO**

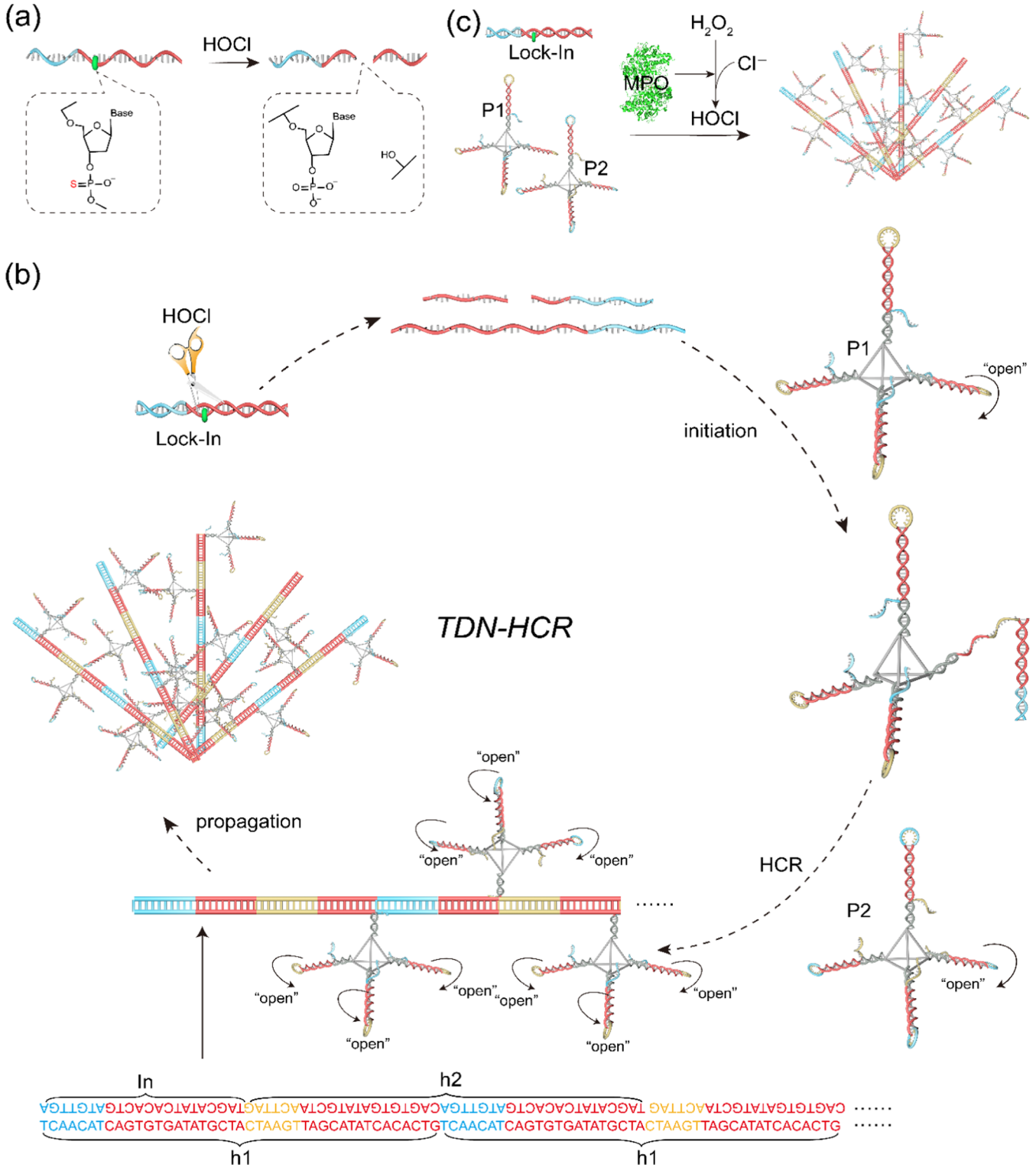


shown to have many advantages, such as high sensitivity, fast response time, and simple operation.[16,17] However, the use of fluorescent probes for HOCl has some limitations:[18] (1) The ultrahigh sensitivity of the probes to reactive oxygen species, such as superoxide anion radical, hydroxyl radical, and hydrogen peroxide, increases the risk of oxidation in air, which is not favorable for long-term storage. (2) The probes are difficult to quantitatively measure the actual concentration of HOCl because of intensity-based fluorescence output, which can cause artifacts due to bleaching, focus changes, laser intensity and probe concentration variations, etc. (3) Most of the fluorescent probes require complex multistep synthesis and have some obvious disadvantages such as low yield, susceptibility to interference from probe concentration,


https://doi.org/10.1021/acs.analchem.1c04113
Anal. Chem. 2021, 93, 16231−16239

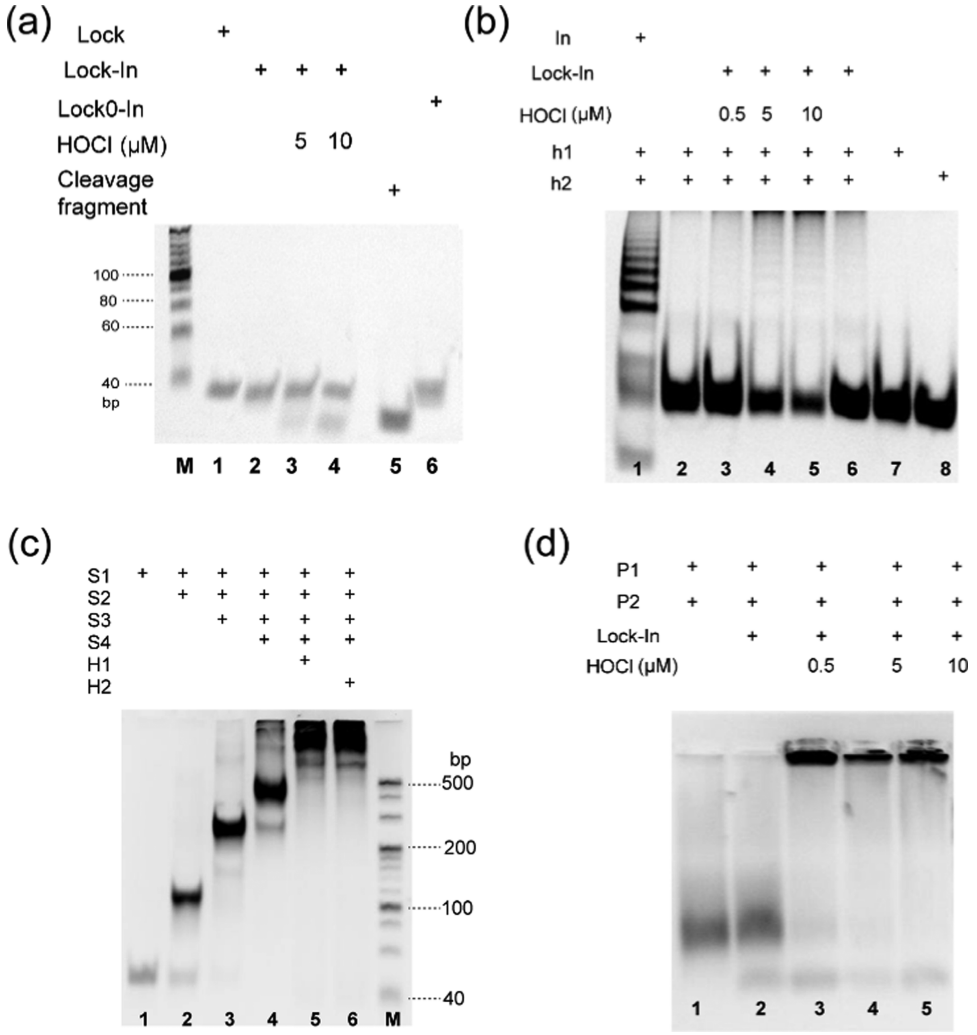


**Figure 1.** Electrophoretic characterization. (a) HOCl cleaved PS-modified **Lock-In**. Condition: [**Lock**] = [**Lock-In**] = [**Lock0-In**] = [Cleavage fragment1] = 2 $\mu$M, 1× PBS buffer, 37 °C for 1 h, and PAGE (10%). (b) HOCl initiated the traditional HCR. Condition: [**Lock**] = [**Lock-In**] = 2 $\mu$M, [**h1**] = [**h2**] = 2 $\mu$M, 1× PBS buffer, 37 °C for 4 h, and PAGE (10%). (c) TDN-based building blocks (**P1** and **P2**). Condition: [S1] = [S2] = [S3] = [S4] = 1 $\mu$M, [**H1**] = [**H2**] =4 $\mu$M, TM buffer, 95 °C for 5 min, then cooling to 4 °C within 1 min, and PAGE (6%). (d) HOCl initiated the TDN-mediated HCR. Condition: [**P1**] = [**P2**] = 500 nM, [**H1**] = [**H2**] = 2 $\mu$M, [**Lock-In**] = 2 $\mu$M, 37 °C for 30 min, and AGE (2%).

background fluorescence, and insurmountable toxicity. (4) Previous attempts to develop near-infrared (NIR) fluorescent probes for HOCl were found to be unstable in the presence of HOCl, which makes NIR fluorescent probes very rare.

The introduction of nanotechnology can overcome many limitations of traditional probes, greatly improve the sensitivity and other properties of biosensors, and promote the development of new types of biosensors, which are important for the early diagnosis of cancer and cardiovascular diseases.[19,20] As an emerging class of building blocks of nanomaterials, nucleic acid has the advantages of programmability, compatibility, and good biocompatibility. By introducing chemical modifications, a series of molecules with unnatural backbones or nucleic acid bases can be synthesized. They have achieved remarkable results in terms of probe design. In addition, nucleic acid framework materials (e.g., DNA tetrahedra,[21,22] DNA octahedra,[23] DNA icosahedra,[24] DNA cubes,[25] etc.) have been widely used to design probe scaffolds, improving the sensing performance of the probes, broadening the application range, and promoting the feasibility of DNA probes in clinical practice.[26−30] In this work, we developed an oxidative cleavage-based three-dimensional DNA biosensor for rapid, ratiometric detection of HOCl and MPO in a "one-pot" method (Scheme 1).

Previous studies have shown that modification of a genome in the form of phosphorothioate (PS) is specifically sensitive to the oxidative effects of HOCl. Such dynamic modifications can lead to genomic instability during oxidative stress.[31−33] Thus, when nonbridging oxygen in the nucleic acid structure is modified with PS, the addition of appropriate amounts of HOCl produces cleavage at specific sites (Scheme 1a). Since PS-modified nucleic acids only slightly disrupt the structure of DNA, they do not affect base pairing and retain the programmability of DNA, which makes them highly promising for the development of HOCl-associated probes and biosensors.

In this work, the mechanism of the proposed tetrahedral DNA nanostructure-mediated hybridization chain reaction (TDN-HCR)-based HOCl-sensing strategy is shown in Scheme 1b. HCR is a highly facile and multifunctional enzyme-free nucleic acid isothermal amplification technique. In traditional HCR, a nucleic acid initiator (**In**) triggers the


https://doi.org/10.1021/acs.analchem.1c04113
Anal. Chem. 2021, 93, 16231−16239

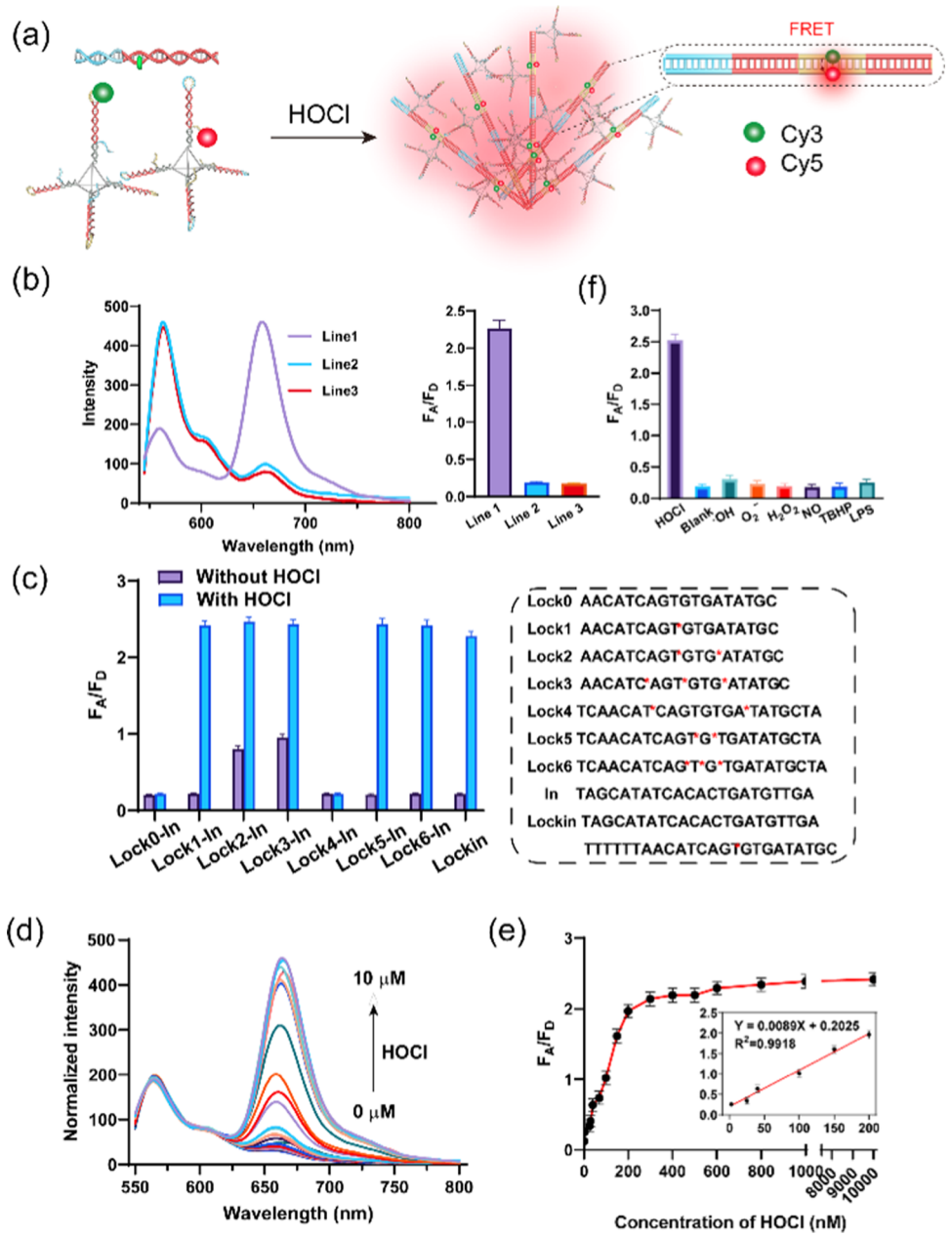


**Figure 2.** (a) Illustration of the TDN-mediated HCR platform for ratiometric fluorescent detection of HOCl. (b) Fluorescence spectra and FRET ratios ($F_A/F_D$) in response to the addition of different components. Line1: **P1** + **P2** + **Lock-In** + HOCl, Line2: **P1** + **P2** + **Lock-In**, and Line3: **P1** + **P2**. (c) Measurement of $F_A/F_D$ in response to different **Locks**. (d) Fluorescence spectra of the biosensor with addition of HOCl (0−10 $\mu$M). (e) HOCl concentration-dependent changes in $F_A/F_D$ vs HOCl concentration (0−10 $\mu$M) and the linear relationship (inset) between $F_A/F_D$ and HOCl concentration in the range of 0−200 nM. (f) $F_A/F_D$ changes of TDN-HCR toward HOCl (500 nM) and other analytes (5 $\mu$M). Conditions: [**P1**] = [**P2**] = 50 nM, [$\mathbf{H1}^{Cy3}$] = [$\mathbf{H2}^{Cy5}$] = 200 nM, [**Lock-In**] = 500 nM, [HOCl] = 1 $\mu$M, and reaction at 37 °C for 30 min. $\lambda_{ex}$ = 548 nm.

alternate opening of two hairpin probes (**h1** and **h2**), giving a long linear double-stranded assembly, accompanied by signal output such as fluorescence resonance energy transfer (FRET). However, traditional HCR often suffers from the shortcomings such as weak probe biostability, slow reaction kinetics, and limited signal amplification efficiency. To address these shortcomings, we developed the TDN-HCR strategy by anchoring **h1** and **h2** to the four vertices of the TDN. To complement the protruding ends of the four strands of TDN, **H1** and **H2** were designed by adding $T_{22}G_2$ to **h1** and **h2**, respectively. Subsequently, two sets of TDN hairpin units (**P1** and **P2**) can be obtained by attaching **H1** and **H2** to the four vertices of the TDN. The addition of **In** opens **H1** in **P1**, and the released sequence can further open **H2** in **P2** to form an **H1**/**H2** complex, which eventually assembles to form a hyperbranched nucleic acid structure. Next, we designed the lock chain (**Lock**) containing PS modification based on the sequence characteristics of **In**. Without the addition of HOCl, **Lock** and **In** form a duplex (**Lock-In**) to make HCR impossible. When different concentrations of HOCl were added, the position of PS in **Lock** was cleaved and the **Lock** structure was unstable, releasing **In** from the complex (**Lock-In**) and thus initiating the HCR to detect HOCl. The oligonucleotides above are listed in Table S1.

To achieve the proposed HOCl-sensing performance, the $T_m$ values of **Lock-In**, fragment1/**In**, and fragment2/**In** were


https://doi.org/10.1021/acs.analchem.1c04113
Anal. Chem. 2021, 93, 16231−16239

first evaluated by software. The $T_m$ value of **Lock-In** was 59.4 °C, which was stable enough at 37 °C (Figure S1). After being cut by hypochlorous acid, the $T_m$ values of two parts fragment1/**In** (AACATCAGT vs TAGCATATCACACT-GATGTTGA) and fragment2/**In** (GTGATATGC vs TAG-CATATCACACTGATGTTGA) were 36.2 and 30.9 °C, respectively, resulting in releasing **In** from the complex (**Lock-In**) at 37 °C. Then, the secondary structures of the hairpins (**h1** and **h2**), **In**, **Lock**, and their double-stranded nucleic acids were also evaluated. Under the condition of PBS buffer (pH 7.4, containing 137 mM NaCl), the preferential secondary structures and corresponding thermodynamic parameters of **h1**, **h2**, **In**, **Lock-In** duplex, **h1**/**In** duplex, and **h1**/**h2** duplex were analyzed by Nupack software. All of the hairpins showed highly negative Gibbs free energy ($\Delta G$), indicating that they were stable and had few other secondary structures. The difference in $\Delta G$ for the HCR indicates that the hybridization reaction can proceed in the presence of **In**, demonstrating the thermodynamic feasibility of the HCR process.

Then, the feasibility of the proposed sensing strategy was preliminarily evaluated by polyacrylamide gel electrophoresis (PAGE) and agarose gel electrophoresis (AGE). (1) **Lock** cleavage by HOCl: As shown in Figure S2, a new band with a faster migration rate appeared when fluorescently labeled **Lock** was incubated with different concentrations of HOCl. The ratio of the cleavage reaction was highly HOCl concentration-dependent. With the increase of HOCl concentration to 0.5 $\mu$M, the **Lock** cleavage product could be clearly observed in PAGE gel. (2) **Lock-In** cleavage by HOCl: As shown in Figure 1a, **Lock** hybridized with **In** to form a stable **Lock-In** duplex with a slower migration rate than **Lock**. Meanwhile, when **Lock-In** was treated with HOCl, a new band corresponding to the cleavage fragment of fluorescently labeled **Lock** appeared and showed a HOCl-dependent intensity increase, indicating that the **Lock** strand was cleaved and released from the **Lock-In** duplex. (3) HOCl-triggered traditional HCR: **h1**, **h2**, and **h1** + **h2** exhibited a single DNA band (Figure 1b, lanes 2, 7, and 8, respectively). Upon the addition of **In**, long nicked double-stranded DNA bands resembling the alternating copolymer can be clearly seen on the gel (lane 1). The HCR process was inhibited when **In** was replaced by **Lock-In** (lane 6). When **In** was released from **Lock** by HOCl, the HCR process can proceed automatically again. It can be clearly seen from the results of lanes 3−5 that the presence of HOCl was necessary for the initiation of the HCR process. In addition to the concentration of HOCl, the concentration of **Lock-In** also significantly affects the reactivity of HCR. The HCR is also highly sensitive to **Lock-In** and improves with the increase of concentration (Figure S3). (4) HOCl-initiated TDN-HCR: The successful assembly of **H1** and **H2** on TDN vertices was clearly verified by PAGE analysis (Figure 1c). The resultant **P1** and **P2** can replace **h1** and **h2**, respectively, to perform HOCl-initiated TDN-HCR. Similar DNA bands were given by **P1**/**P2** and **P1**/**P2**/**Lock-In** mixtures (Figure 1d, lanes 1 and 2), suggesting that **Lock-In** would not spontaneously initiate TDN-HCR. In the presence of HOCl, however, a large-sized HCR product (Figure 1d, lanes 3−5) that could not migrate from the loading site was formed, indicating the successful initiation of TDN-HCR by HOCl. It should be noted that even 0.5 $\mu$M HOCl could efficiently initiate TDN-HCR, implying the greatly improved HOCl-sensing performance of TDN-HCR compared to traditional HCR.

The FRET-based ratiometric detection mode is significantly superior to the common fluorophore/quencher system because it can effectively prevent the false-positive signal caused by probe degradation, concentration fluctuation, and excitation light intensity variation. To achieve FRET detection of HOCl in solution, the fluorophore donor Cy3 and the fluorophore acceptor Cy5 were modified at the appropriate positions of **H1** and **H2**, respectively. After successful initiation of TDN-HCR by HOCl, the FRET between Cy3 and Cy5 would change from "off" to "on" state (Figure 2a). Considering that the fluorescence of some fluorochromes is susceptible to reactive oxygen species,[34] the effects of HOCl on the Cy3 and Cy5 fluorescence were first investigated. As shown in Figure S4, the fluorescence of both Cy3 and Cy5 was barely changed when the HOCl concentration was less than 100 $\mu$M. When the HOCl concentration was between 100 and 200 $\mu$M, the fluorescence intensity of both Cy3 and Cy5 decreased, but the intensity ratio between them remained almost unchanged. When the HOCl concentration exceeded 200 $\mu$M, both Cy3 and Cy5 showed greatly decreased fluorescence intensity, and their intensity ratio was also changed greatly. That is, as long as the HOCl concentration is lower than 100 $\mu$M, the Cy3 and Cy5 fluorescence and their ratio will not be disturbed.

To confirm the feasibility of our proposed HOCl-sensing strategy, fluorescence spectra of different systems were recorded. As shown in Figure 2b, identical fluorescence spectra were given by **P1**/**P2** and **P1**/**P2**/**Lock-In** mixtures (Line2 and Line3, respectively). When HOCl was added in the **P1**/**P2**/**Lock-In** mixture, TDN-HCR was successfully initiated, resulting in greatly decreased Cy3 fluorescence and significantly increased Cy5 fluorescence (Line1). The FRET ratio ($F_A/F_D$) with HOCl is about 12.7-fold higher than that of the blank control without HOCl ($F_A$ is the Cy5 fluorescence at 665 nm and $F_D$ is the Cy3 fluorescence at 561 nm, $\lambda_{ex}$ = 548 nm).

Having demonstrated the feasibility for ratiometric detection of HOCl, we optimized the biosensor design and some important experimental conditions to achieve the best assay performance. First, the optimal **Lock** was selected (Figure 2c). An ideal **Lock** should stably hybridize with **In** and remain silent in the absence of HOCl but can be rapidly cleaved by HOCl to release **In** and thus trigger the subsequent HCR process. Therefore, the numbers and sites of PS modification in **Lock** were carefully selected. Four **Lock** strands with the same length but different numbers of PS modifications (**Lock0**, **Lock1**, **Lock2**, and **Lock3**, in which the PS modification sites are 0, 1, 2, and 3, respectively) were compared. Due to the lack of PS modification, the **Lock0-In** duplex showed no response to HOCl and cannot initiate HOCl-dependent TDN-HCR. On the contrary, **Lock1-In**, **Lock2-In**, and **Lock3-In** could respond to HOCl, giving greatly increased $F_A/F_D$. However, when the number of modification sites was two or more, the background signal increased sharply. It was reported that compared to the unmodified duplex, $T_m$ decreases by 0.65 °C on average for each PS site.[35] The effect of PS modification on duplex instability can be overcome by increasing the length of the duplex. When the length of the **Locks** (**Lock4**−**6**) was extended and the PS modification sites were gradually added, the HCR remained silent in the absence of HOCl. Among them, **Lock5-In** and **Lock6-In** can be rapidly cleaved by HOCl to release **In** and thus trigger the subsequent HCR process, while **Lock4** cannot. Therefore, the PS modification site should be designed close to the middle of the **Locks**. This


https://doi.org/10.1021/acs.analchem.1c04113
Anal. Chem. 2021, 93, 16231−16239

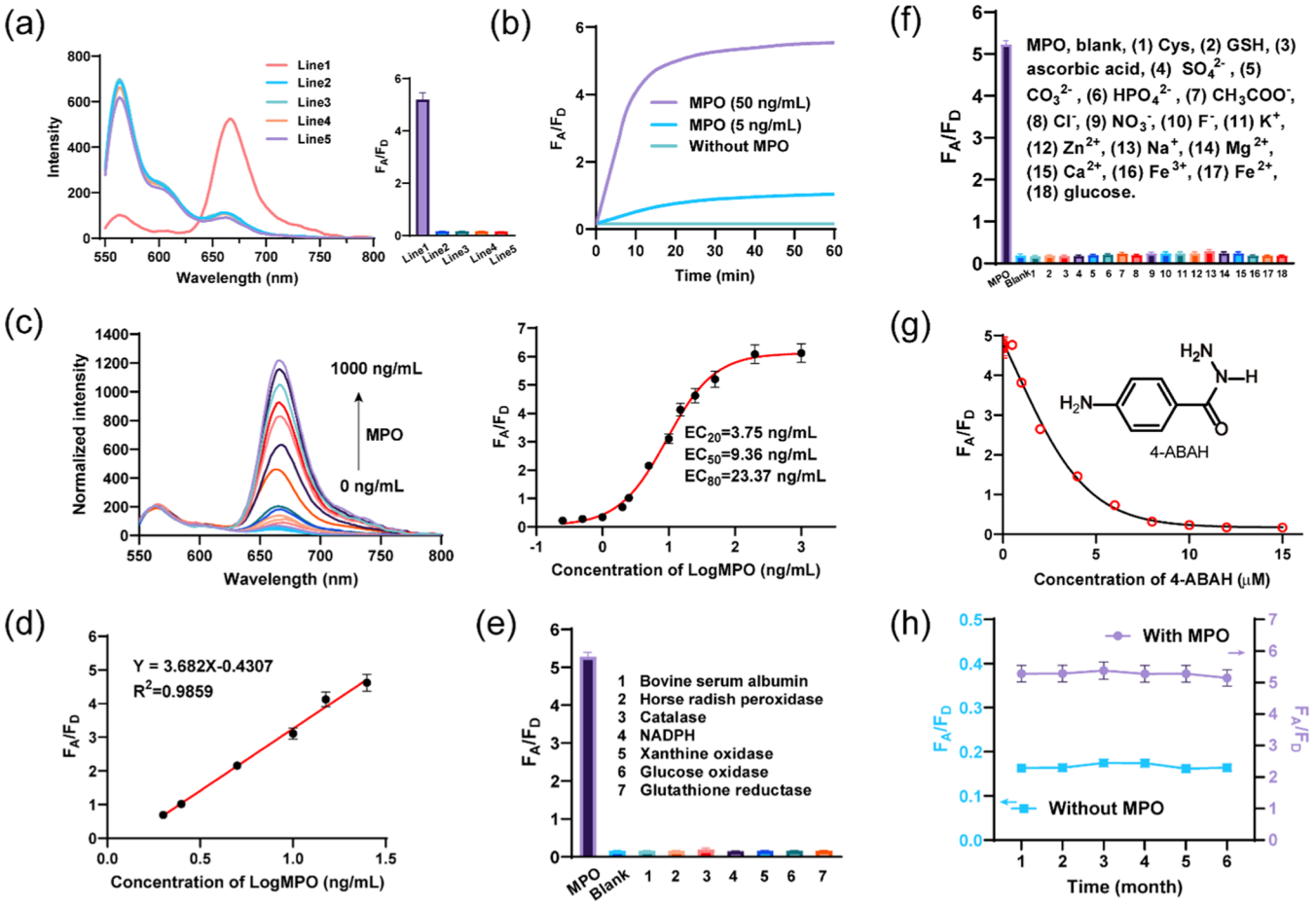


**Figure 3.** (a) Fluorescent spectrum and FRET ratio ($F_A/F_D$) in response to the addition of different components. Line1: **P1** + **P2** + **Lock-In** + MPO + $Cl^-$ + $H_2O_2$, Line2: **P1** + **P2** + **Lock-In** + MPO + $Cl^-$, Line3: **P1** + **P2** + **Lock-In** + MPO + $H_2O_2$, Line4: **P1** + **P2** + **Lock-In** + $Cl^-$ + $H_2O_2$, and Line5: **P1** + **P2** + **Lock-In**. (b) Time dependence of $F_A/F_D$ upon the addition of MPO. (c) MPO concentration-dependent changes in fluorescence spectra and $F_A/F_D$ in the range of 0−1000 ng/mL. (d) The linear relationship between $F_A/F_D$ and the logarithm of MPO concentration in the range of 2−25 ng/mL. (e) $F_A/F_D$ changes of the biosensor toward MPO (50 ng/mL) and other analytes (500 ng/mL). (f) Anti-interference ability of the biosensor to common physiological substance. (g) Effect of different concentrations of 4-ABAH on the chlorination activity of MPO. (h) Long-time stability of the biosensor over 6 months. (e−h) The concentration of MPO was 50 ng/mL. Conditions: [**P1**] = [**P2**] = 50 nM, [$\mathbf{H1}^{Cy3}$] = [$\mathbf{H2}^{Cy5}$] = 200 nM, [**Lock-In**] = 200 nM, [$H_2O_2$] = [$Cl^-$] = 100 $\mu$M, PB 6.0, and reaction at 37 °C for 30 min. $\lambda_{ex}$ = 548 nm.

allows for the maximum possible release of **In** after the duplex is cut by HOCl. Besides, the **Lock** and **In** can also be grouped into one strand, such as Lockin. **Lock**, referred to as **Lock1**, was taken as an example for subsequent HOCl detection analysis.

Next, using $R/R_0$ as the criterion ($R$ and $R_0$ are $F_A/F_D$ with and without HOCl, respectively), operation conditions for HOCl quantitation, including the concentration and ratio of DNA probes (**P1**, **P2**, and **Lock-In**), buffer type and pH, and reaction time, were optimized (Figures S5−S9). Among them, probe concentration, ratio, and reaction time have significant effects on the reaction, while the buffer type and pH showed slight effects. After optimization, 50 nM **P1**, 50 nM **P2**, 500 nM **Lock-In**, and a reaction time of 30 min were chosen for HOCl detection in the following experiments.

Under the optimized conditions, the sensitivity of the proposed HOCl-sensing platform was evaluated. The $F_A/F_D$ value gradually increased with the HOCl concentration from 0 to 10 $\mu$M (Figure 2d), and a linear relationship ($R^2$ = 0.9918) was obtained in the range of 2.5−200 nM (Figure 2e). The regression equation was $Y = 0.0089X + 0.2025$ (where $Y$ and $X$ represent $F_A/F_D$ and HOCl concentrations, respectively), and the limit of detection (LOD) was estimated to be 0.8 nM according to the $3\sigma/S$ rule ($\sigma$ represents the standard deviation of the blank control ($N$ = 10) and $S$ is the slope of the calibration curve). Notably, compared to other methods based on colorimetric or fluorescent detection, our biosensor gives the lowest LOD to our knowledge (Table S2). Notably, although the sensing process consists of HOCl-triggered **Lock-In** cleavage and released **In**-initiated TDN-HCR, the operation of these two steps can be combined so that the entire HOCl sensing is done in the "one-pot" mode, which greatly simplifies the sensing operation.

Biosensors with high selectivity and anti-interference properties are known to facilitate accurate detection of HOCl due to the abundance of reactive oxygen species and reduced species in biological systems. We further investigated the selectivity of the biosensor for HOCl against other potentially interfering analytes. As shown in Figure 2f, only HOCl contributed to a significant enhancement of $F_A/F_D$ compared to other interfering analytes that exhibited negligible changes in $F_A/F_D$ even at 10 times higher concentrations.


https://doi.org/10.1021/acs.analchem.1c04113
Anal. Chem. 2021, 93, 16231−16239

These results confirm that our biosensor can achieve highly selective detection of HOCl in complex biological systems.

Although our proposed strategy can detect HOCl in solution, the short lifetime of HOCl in biological samples makes it difficult to develop liquid biopsy kits based on HOCl detection. In fact, quantitative testing of MPO has greater clinical utility.[36,37] Under physiological conditions, MPO mediates the peroxidation of the chloride ion ($Cl^-$) by $H_2O_2$ to produce HOCl. Therefore, our proposed strategy can be easily extended to monitor MPO activity (Figure 1c). In the presence of $Cl^-$ and $H_2O_2$, the addition of MPO could greatly increase the FRET signal of the sensing system, demonstrating the feasibility of our method for MPO detection. On the contrary, almost no FRET signal change was observed for the sensing system lacking $Cl^-$, $H_2O_2$, or MPO, demonstrating the proposed sensing mechanism. That is, MPO catalyzes the oxidation of $Cl^-$ to produce HOCl, which then initiates TDN-HCR to give enhanced FERT signal output (Figure 3a).

To obtain the best MPO-sensing performance, some critical experimental conditions were optimized using $R/R_0$ as the criterion, including reaction temperature, concentrations of $Cl^-$, $H_2O_2$, and **Lock-In**, buffer type and pH, and reaction time (Figures 3b and S10−S14). Since the optimal reaction temperatures for MPO and TDN-HCR are 25 and 37 °C, respectively, we examined the effects of three temperatures (25, 30, and 37 °C) on the detection of MPO and finally selected 37 °C as the reaction temperature. In the MPO−$H_2O_2$−$Cl^-$ system, the presence of $H_2O_2$ and $Cl^-$ is crucial for the detection of MPO, and the experimental results showed that the biosensor gave excellent MPO-sensing performance in a wide range of $Cl^-$ and $H_2O_2$ concentrations. Besides, the pH, reaction time, and **Lock-In** concentration also had significant effects on the sensing performance. Finally, we chose 37 °C, 200 nM **Lock-In**, 100 $\mu$M $Cl^-$, 100 $\mu$M $H_2O_2$, PB buffer with pH 6.0, and a reaction time of 30 min for the detection of MPO.

Under optimized conditions, the MPO-sensing performance of the proposed method was evaluated. As shown in Figure 3c, the FRET signal was closely related to the MPO concentration. The $F_A/F_D$ value showed an S-shaped curve with MPO in the concentration range of 0−1000 ng/mL. $EC_{20}$, $EC_{50}$, and $EC_{80}$ (maximal effective concentration, EC) refer to the concentrations of MPO, which induce 20, 50, and 80% responses of the maximum effect. In the range of 2−25 ng/mL, the $F_A/F_D$ showed a linear correlation ($R^2$ = 0.9859) with the logarithmic of MPO concentrations (Figure 3d). The regression equation was $Y = 3.682X - 0.4307$, where $Y$ and $X$ represent the $F_A/F_D$ ratio and the logarithmic of MPO concentration, respectively. The LOD was estimated to be 3.75 ng/mL, better than or comparable to the reported colorimetric, fluorescent, and electrochemical detection methods. Although showing a higher LOD than the immunoassay method (Table S3), the greatly simplified operations and significantly shortened time make our method more suitable for practical applications.

Then, the specificity of MPO detection was investigated by detecting several other common enzymes (horseradish peroxidase, catalase, xanthine oxidase, glucose oxidase, and glutathione reductase), bovine serum albumin, various biologically relevant molecules, such as metal ions, anions, redox substances, amino acids, and glucose, and other reactive oxygen species. As shown in Figures 3e,f and S15, none of the tested biomolecules and ions gave positive FRET signals compared to the blank control.

Elevated MPO concentration and activity are associated with many pathological factors that lead to the onset and progression of inflammatory events. Recent studies have shown that MPO can serve as an important diagnostic biomarker and therapeutic target.[38,39] Therefore, screening for active compounds that can effectively inhibit MPO activity and thus attenuate the inflammatory response is the focus of current research.[2,40,41] To evaluate the potential of biosensors in screening for MPO inhibitors, we used 4-aminobenzoic acid hydrazide (4-ABAH), a drug widely used as an irreversible inhibitor of MPO, as a model. As shown in Figure 3g, the $F_A/F_D$ ratio decreased with the increasing concentration of 4-ABAH (0−15 $\mu$M). The half-maximal inhibitory concentration ($IC_{50}$) was calculated to be 0.77 $\mu$M, which is similar to those reported in recent studies.[8,16,42] This result suggests that our proposed biosensor can be used to screen MPO inhibitors and evaluate their inhibitory activities, showing great potential in the development of anti-inflammatory drugs.

A stable and reliable biosensor is essential for the development of a diagnostic kit. Then, the proposed sensing systems were kept at 4 °C for different times, and their MPO detection capability was followed up for 6 months. As shown in Figure 3h, the background value of the sensing system was barely changed from the beginning to after 6 months, accompanied by comparable MPO-sensing performance with a relative standard deviation of about 1.5% for the experimental data, indicating that the biosensor has good stability even after long-term storage.

The biosensor was further used to detect MPO activity in real samples. Plasma was selected as the real sample model. First, the effect of the plasma dilution ratio on MPO detection was tested. The same concentration of HOCl or MPO was added to samples at different dilutions, and it was found that approximately 100-fold diluted plasma had no significant effect on the MPO detection. MPO detection is impossible in 10-fold diluted plasma, which even could not be counteracted by adding more $H_2O_2$ to neutralize the reducing substances in the sensing system (Figure S16). Next, different concentrations of MPO were added to 100-fold diluted plasma samples, and the recoveries were calculated by comparing the measured MPO activity with the amount added. For comparison, MPO spiked in real samples was also determined by a commercial test kit. The recoveries of MPO in plasma determined by our method ranged from 95.6 to 102.3% with relative standard deviations of 2.9−14.2%, respectively, which were consistent with the results of the commercial kit (Table 1). This indicates that our proposed method has good precision and high accuracy. Finally, we applied our biosensor to other three real samples: serum, cell lysate, and saliva (Table S4). The results suggested that the biosensor can be used for the quantitative determination of MPO in complex biological samples.

**Table 1. Recovery Studies of MPO in Real Samples**

| samples | added (ng/mL) | measured (ng/mL) | recovery (%) | RSD (%) | kit assay (ng/mL) |
|---|---|---|---|---|---|
| 1 | 2.5 | 2.558 | 102.3 | 4.4 | 2.741 |
| 2 | 10 | 10.066 | 100.6 | 14.2 | 10.367 |
| 3 | 20 | 19.123 | 95.6 | 2.9 | 23.568 |

Abnormalities in MPO lead to individual differences in susceptibility to certain diseases and are closely associated with the occurrence and development of many human diseases, so


https://doi.org/10.1021/acs.analchem.1c04113
Anal. Chem. 2021, 93, 16231−16239

its rapid detection is of increasing interest to scholars both domestically and internationally. Our biosensor can also combine with a low-cost portable detection device to achieve the point-of-care testing (POCT) of MPO. Therefore, a fluorescent/quencher pair (Alexa Fluor 488/BHQ1) was used to label **H1**. The fluorescence of Alexa Fluor 488 was quenched due to the close contact between the fluorophore and the quencher in the hairpin structure. MPO can trigger the TDN-HCR between **P1** and **P2**, leading to the opening of the hairpin structure, which restores the fluorescence of Alexa Fluor 488. By utilizing a handheld UV lamp to irradiate the sensing systems, bright green fluorescence was given by the four MPO-positive real samples (Figure 4). The detection

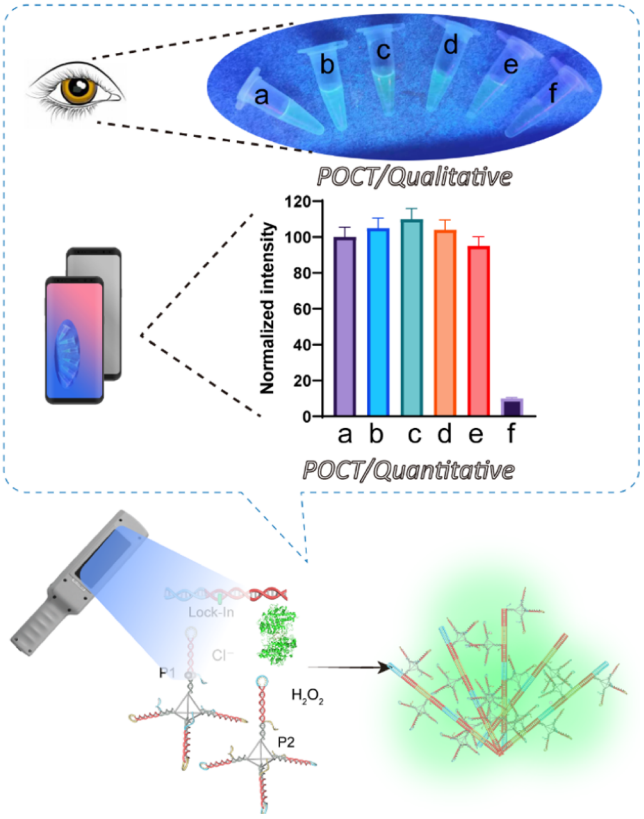


**Figure 4.** Fluorescence photographs and histogram of the fluorescence intensity of six samples with or without MPO. a: MPO added in PBS 7.4, b: MPO added in plasma, c: MPO added in serum, d: MPO added in cell lysate, e: MPO added in saliva, and f: PBS without MPO. Conditions: [**P1**] = [**P2**] = 50 nM, [$\mathbf{H1}^{FQ}$] = [**H2**] = 200 nM, [**Lock-In**] = 200 nM, [$H_2O_2$] = [$Cl^-$] = 100 $\mu$M, PB 6.0, and reaction at 37 °C for 30 min. $\lambda_{ex}$ = 548 nm.

results can be judged by the naked eye or a smartphone, which can grade fluorescence intensity semiquantitatively. That is, our proposed method can be used for developing portable MPO detection kits that can even be used in resource-short or remote areas.

In summary, we constructed a novel and facile nucleic acid biosensor based on PS-modified oxidative cleavage to provide a new scheme for the detection of HOCl and MPO. The fluorescent method established in this study is the lowest among the methods reported so far and used for spiked detection in complex matrices. Our design has the following advantages: (1) Fast, controllable preparation and one-pot detection: The probe construction can be completed in only 5 min. No complicated reaction conditions and operations have been required by the PS site cleavage reaction. Compared with the existing methods that usually take several hours, the detection time is less than 30 min, which greatly improves the efficiency of sensor detection. (2) Ratiometric detection: In addition to preventing false-positive signals, the ratiometric assay has the advantage of quantification of analytes. The biosensor is resistant to the pH range, buffer types, and matrix. (3) Stable signal output and long storage: the performance of the sensing system was barely changed within 6 months, indicating that the biosensor has good stability even after long-term storage. (4) Simplicity and security: The biosensor does not involve complex organic synthesis, easily degradable enzymes, trained operators, expensive instrumentation, and dedicated laboratory space, which makes it possible to obtain reliable detection results even in resource-limited environments. Moreover, no reagents contain hazardous substances, which are not user-friendly or environmentally friendly. (5) Strong versatility: The HCR-based signal amplification circuit design can be extended to other signal amplification strategies. Therefore, our work not only can be widely used in research fields related to biosensors and molecular diagnostics but also has great potential for commercial applications.

## ■ ASSOCIATED CONTENT

### Supporting Information

The Supporting Information is available free of charge at https://pubs.acs.org/doi/10.1021/acs.analchem.1c04113.

Additional experimental details; materials; methods; and figures as mentioned in the text (PDF)

## ■ AUTHOR INFORMATION


### Corresponding Author

**De-Ming Kong** − *State Key Laboratory of Medicinal Chemical Biology, Tianjin Key Laboratory of Biosensing and Molecular Recognition, Research Centre for Analytical Sciences, College of Chemistry, Nankai University, Tianjin 300071, China;* orcid.org/0000-0002-9216-8040; Email: kongdem@nankai.edu.cn

### Authors

**Jing Wang** − *State Key Laboratory of Medicinal Chemical Biology, Tianjin Key Laboratory of Biosensing and Molecular Recognition, Research Centre for Analytical Sciences, College of Chemistry, Nankai University, Tianjin 300071, China;* orcid.org/0000-0002-9100-6429

**Jia-Yi Ma** − *State Key Laboratory of Medicinal Chemical Biology, Tianjin Key Laboratory of Biosensing and Molecular Recognition, Research Centre for Analytical Sciences, College of Chemistry, Nankai University, Tianjin 300071, China*

**Dong-Xia Wang** − *State Key Laboratory of Medicinal Chemical Biology, Tianjin Key Laboratory of Biosensing and Molecular Recognition, Research Centre for Analytical Sciences, College of Chemistry, Nankai University, Tianjin 300071, China*

**Bo Liu** − *State Key Laboratory of Medicinal Chemical Biology, Tianjin Key Laboratory of Biosensing and Molecular Recognition, Research Centre for Analytical Sciences, College of Chemistry, Nankai University, Tianjin 300071, China*

**Xiao Jing** − *State Key Laboratory of Medicinal Chemical Biology, Tianjin Key Laboratory of Biosensing and Molecular*




https://doi.org/10.1021/acs.analchem.1c04113
Anal. Chem. 2021, 93, 16231−16239

*Recognition, Research Centre for Analytical Sciences, College of Chemistry, Nankai University, Tianjin 300071, China*

**Dan-Ye Chen** − *State Key Laboratory of Medicinal Chemical Biology, Tianjin Key Laboratory of Biosensing and Molecular Recognition, Research Centre for Analytical Sciences, College of Chemistry, Nankai University, Tianjin 300071, China*

**An-Na Tang** − *State Key Laboratory of Medicinal Chemical Biology, Tianjin Key Laboratory of Biosensing and Molecular Recognition, Research Centre for Analytical Sciences, College of Chemistry, Nankai University, Tianjin 300071, China;* orcid.org/0000-0001-5411-9216

Complete contact information is available at: https://pubs.acs.org/10.1021/acs.analchem.1c04113

### Author Contributions

The manuscript was written through contributions of all authors. All authors have given approval to the final version of the manuscript.

### Notes

The authors declare no competing financial interest.

## ■ ACKNOWLEDGMENTS

This work was supported by the National Key R&D Program of China (2019YFA0210103) and the National Natural Science Foundation of China (Nos. 22074068 and 21874075). The authors also thank all of the reviewers for the constructive comments.

## ■ REFERENCES

(1) Rashid, I.; Maghzal, G. J.; Chen, Y. C.; Cheng, D.; Talib, J.; Newington, D.; Ren, M.; Vajandar, S. K.; Searle, A.; Maluenda, A.; Lindstedt, E. L.; Jabbour, A.; Kettle, A. J.; Bongers, A.; Power, C.; Michaelsson, E.; Peter, K.; Stocker, R. *Eur. Heart J.* **2018**, *39*, 3301−3310.

(2) Huang, J.; Milton, A.; Arnold, R. D.; Huang, H.; Smith, F.; Panizzi, J. R.; Panizzi, P. *J. Leukocyte Biol.* **2016**, *99*, 541−548.

(3) Bassegoda, A.; Ferreres, G.; Perez-Rafael, S.; Hinojosa-Caballero, D.; Torrent-Burgues, J.; Tzanov, T. *Talanta* **2019**, *194*, 469−474.

(4) Wang, C.; Keliher, E.; Zeller, M. W. G.; Wojtkiewicz, G. R.; Aguirre, A. D.; Buckbinder, L.; Kim, H. Y.; Chen, J.; Maresca, K.; Ahmed, M. S.; Motlagh, N. J.; Nahrendorf, M.; Chen, J. W. *Proc. Natl. Acad. Sci. U.S.A.* **2019**, *116*, 11966−11971.

(5) Hajnsek, M.; Schiffer, D.; Harrich, D.; Koller, D.; Verient, V.; vd Palen, J.; Heinzle, A.; Binder, B.; Sigl, E.; Sinner, F.; Guebitz, G. M. *Sens. Actuators, B* **2015**, *209*, 265−274.

(6) Liu, B.; Lu, L. *Microchim. Acta* **2019**, *186*, No. 262.

(7) Guo, J.; Tao, H.; Dou, Y.; Li, L.; Xu, X.; Zhang, Q.; Cheng, J.; Han, S.; Huang, J.; Li, X.; Li, X.; Zhang, J. *Mater. Today* **2017**, *20*, 493−500.

(8) Zhang, N.; Francis, K. P.; Prakash, A.; Ansaldi, D. *Nat. Med.* **2013**, *19*, 500−505.

(9) Gross, S.; Gammon, S. T.; Moss, B. L.; Rauch, D.; Harding, J.; Heinecke, J. W.; Ratner, L.; Piwnica-Worms, D. *Nat. Med.* **2009**, *15*, 455−461.

(10) Bekhit, M.; Gorski, W. *Anal. Chem.* **2019**, *91*, 3163−3169.

(11) Tao, H.; Guo, J.; Ma, Y.; Zhao, Y.; Jin, T.; Gu, L.; Dou, Y.; Liu, J.; Hu, H.; Xiong, X.; Zhang, J. *ACS Nano* **2020**, *14*, 11083−11099.

(12) You, Y.; Cheng, S.; Zhang, L.; Zhu, Y.; Zhang, C.; Xian, Y. *Anal. Chem.* **2020**, *92*, 5091−5099.

(13) Rodríguez, E.; Nilges, M.; Weissleder, R.; Chen, J. W. *J. Am. Chem. Soc.* **2010**, *132*, 168−177.

(14) Wang, C.; Pulli, B.; Jalali Motlagh, N.; Li, A.; Wojtkiewicz, G. R.; Schmidt, S. P.; Wu, Y.; Zeller, M. W. G.; Chen, J. W. *Theranostics* **2019**, *9*, 7525−7536.

(15) He, X.; Chen, H.; Xu, C.; Fan, J.; Xu, W.; Li, Y.; Deng, H.; Shen, J. *J. Hazard. Mater.* **2020**, *388*, No. 122029.

(16) Thekkan, S.; Jani, M. S.; Cui, C.; Dan, K.; Zhou, G.; Becker, L.; Krishnan, Y. *Nat. Chem. Biol.* **2019**, *15*, 1165−1172.

(17) Kwon, N.; Kim, D.; Swamy, K. M. K.; Yoon, J. *Coord. Chem. Rev.* **2021**, *427*, No. 213581.

(18) Wu, D.; Chen, L.; Xu, Q.; Chen, X.; Yoon, J. *Acc. Chem. Res.* **2019**, *52*, 2158−2168.

(19) Ouyang, M.; Tu, D.; Tong, L.; Sarwar, M.; Bhimaraj, A.; Li, C.; Cote, G. L.; Di Carlo, D. *Biosens. Bioelectron.* **2021**, *171*, No. 112621.

(20) Wang, Q.; Wang, J.; Huang, Y.; Du, Y.; Zhang, Y.; Cui, Y.; Kong, D.-m. *Biosens. Bioelectron.* **2021**, No. 113739.

(21) Zhang, J.; Guo, Y.; Ding, F.; Pan, G.; Zhu, X.; Zhang, C. *Angew. Chem., Int. Ed.* **2019**, *58*, 13794−13798.

(22) Zhu, J.; Zhang, M.; Gao, Y.; Qin, X.; Zhang, T.; Cui, W.; Mao, C.; Xiao, D.; Lin, Y. *Signal Transduction Targeted Ther.* **2020**, *5*, No. 120.

(23) Wang, W.; Chen, S.; An, B.; Huang, K.; Bai, T.; Xu, M.; Bellot, G.; Ke, Y.; Xiang, Y.; Wei, B. *Nat. Commun.* **2019**, *10*, No. 1067.

(24) Ma, Y.; Wang, Z.; Ma, Y.; Han, Z.; Zhang, M.; Chen, H.; Gu, Y. *Angew. Chem., Int. Ed.* **2018**, *57*, 5389−5393.

(25) Chidchob, P.; Offenbartl-Stiegert, D.; McCarthy, D.; Luo, X.; Li, J.; Howorka, S.; Sleiman, H. F. *J. Am. Chem. Soc.* **2019**, *141*, 1100−1108.

(26) Wang, Y.-X.; Wang, D.-X.; Wang, J.; Du, Y.-C.; Cui, Y.-X.; Tang, A.-N.; Jiang, H.-X.; Kong, D.-M. *Sens. Actuators, B* **2021**, *330*, No. 129335.

(27) Wang, J.; Wang, D. X.; Ma, J. Y.; Wang, Y. X.; Kong, D. M. *Chem. Sci.* **2019**, *10*, 9758−9767.

(28) Wang, D. X.; Wang, J.; Cui, Y. X.; Wang, Y. X.; Tang, A. N.; Kong, D. M. *Anal. Chem.* **2019**, *91*, 13165−13173.

(29) Wang, J.; Ma, J. Y.; Wang, D. X.; Liu, B.; Tang, A. N.; Kong, D. M. *Chem. Commun.* **2021**, *57*, 6760−6763.

(30) Wang, D. X.; Wang, J.; Wang, Y. X.; Du, Y. C.; Huang, Y.; Tang, A. N.; Cui, Y. X.; Kong, D. M. *Chem. Sci.* **2021**, *12*, 7602−7622.

(31) Kellner, S.; DeMott, M. S.; Cheng, C. P.; Russell, B. S.; Cao, B.; You, D.; Dedon, P. C. *Nat. Chem. Biol.* **2017**, *13*, 888−894.

(32) Xiao, L.; Gu, C.; Xiang, Y. *Angew. Chem., Int. Ed.* **2019**, *58*, 14167−14172.

(33) Hu, Z.; Yang, J.; Xu, F.; Sun, G.; Pan, X.; Xia, M.; Zhang, S.; Zhang, X. *J. Am. Chem. Soc.* **2021**, *143*, 12361−12368.

(34) Jia, X.; Chen, Q.; Yang, Y.; Tang, Y.; Wang, R.; Xu, Y.; Zhu, W.; Qian, X. *J. Am. Chem. Soc.* **2016**, *138*, 10778−10781.

(35) Saran, R.; Huang, Z.; Liu, J. *Coord. Chem. Rev.* **2021**, *428*, No. 213624.

(36) Monogioudi, E.; Hutu, D. P.; Martos, G.; Sheldon, J.; Schimmel, H.; Meroni, P. L.; Zegers, I. *Clin. Chim. Acta* **2017**, *467*, 48−50.

(37) Seren, S.; Derian, L.; Keleş, I.; Guillon, A.; Lesner, A.; Gonzalez, L.; Baranek, T.; Si-Tahar, M.; Marchand-Adam, S.; Jenne, D. E.; et al. *Eur. Respir. J.* **2021**, *57*, No. 2003755.

(38) Kazimli, A. V.; Ryzhkov, A. V.; Goncharova, N. S.; Naymushin, A. V.; Moiseeva, O. M. *Eur. Heart J.* **2013**, *34*, No. P332.

(39) Senders, M. L.; Mulder, W. J. M. *Eur. Heart J.* **2018**, *39*, 3311−3313.

(40) Tang, L.; Wang, Z.; Mu, Q.; Yu, Z.; Jacobson, O.; Li, L.; Yang, W.; Huang, C.; Kang, F.; Fan, W.; Ma, Y.; Wang, M.; Zhou, Z.; Chen, X. *Adv. Mater.* **2020**, *32*, No. 2002739.

(41) Xu, X.; An, H.; Zhang, D.; Tao, H.; Dou, Y.; Li, X.; Huang, J.; Zhang, J. *Sci. Adv.* **2019**, *5*, No. eaat2953.

(42) Kettle, A. J.; Gedye, C. A.; Winterbourn, C. C. *Biochem. J.* **1997**, *321*, 503−508.